

# Dynamics on the ground-state potential surfaces of $H_3$ and its isotopomers from their uv spectra

D. Azinovic, R. Bruckmeier, Ch. Wunderlich,\* and H. Figger†  
*Max-Planck-Institut für Quantenoptik, 85748 Garching, Germany*

G. Theodorakopoulos and I. D. Petsalakis  
*Theoretical and Physical Chemistry Institute, National Hellenic Research Foundation, 48 Vassileos Constantinou Avenue,  
 11635 Athens, Greece*  
 (Received 26 January 1998)

The uv spectra of  $H_3$ ,  $D_2H$ , and  $D_3$  emitted by a neutralized ion beam have been measured in the wavelength range 200–400 nm. The spectra are continuous and show two maxima at 240 and 310 nm. Numerical simulations of the uv spectra, taking *ab initio* potential surfaces and transition moments as a starting point, explain their bimodal structure as arising from radiative decay into the two Jahn-Teller sheets of the ground-state potential surface. Two different lifetimes  $\tau_1$  and  $\tau_2$  for the lower sheet and the upper sheet of the Jahn-Teller adiabatic ground-state surface, respectively, were introduced and varied when fitting the simulated spectra to the experimental ones. These lifetimes have to be interpreted as average values for different vibrational states with angular momentum quantum numbers ranging from 0 to 7. The values are for  $H_3$   $\tau_1=3.5$  fs and  $\tau_2=6.7$  fs, for  $D_2H$ ,  $\tau_1=4.9$  fs and  $\tau_2=8.2$  fs, and for  $D_3$ ,  $\tau_1=5.9$  fs and  $\tau_2=8.7$  fs and the error is estimated to be 0.5 fs. These results are consistent among each other, i.e., they show the expected dependence on the square root of the reduced masses. Furthermore, lifetimes for the uv emitting Rydberg states have been measured. Since lifetimes of Rydberg states of  $H_3$  and its isotopomers are already known from analogous measurements in the visible spectrum, the  $3s$  and  $3d$  states could be identified as the main emitters of the uv radiation. Their mean lifetimes range from about 4 ns for  $H_3$ , 5 ns for  $H_2D$ , and 6 ns for  $D_2H$  to 10 ns for  $D_3$ .  
 [S1050-2947(98)07208-4]

PACS number(s): 33.70.Ca, 82.20.Kh, 31.15.Qg, 82.30.Lp

## I. INTRODUCTION

Spectra of  $H_3$  and its isotopomer  $D_3$  have been measured in the light emitted by a hollow cathode discharge through hydrogen and deuterium, respectively [1]. An important recent improvement of that experimental system is the so-called Cossart-type tube, which is a combination of a hollow cathode and a beam-gas system. Using a Cossart-type tube, the  $H_3$  and  $D_3$  spectra could be observed with hardly any lines of  $H_2$  or  $D_2$  present and it was even possible to distinguish partly between pure ( $H_3$  and  $D_3$ ) and mixed isotopomers ( $H_2D$  and  $D_2H$ ) [2]. Another step forward was the application of the ion-beam method where the ions are mass selected before they are neutralized. Thus the spectra of all isotopomers can be clearly distinguished, with only a few lines of other species present that could lead to ambiguities in the interpretation [3].

Spectra of  $H_3$  and  $D_3$  were measured in the visible and the ir wavelength region [4–6]. Important features of the triatomic molecules  $H_3$  and  $D_3$  have been derived from these spectral bands. It has been shown that these molecules are of the excimer type, i.e., the ground states are dissociative while the excited states are bonding or partly predissociative. The higher states are Rydberg states, i.e., can be approximately classified by quantum numbers  $n$  and  $l$ , like atoms, where  $n$  is the principal quantum number and  $l$  the orbital angular

momentum quantum number.  $H_3$  can be modeled by a  $H_3^+$  core that consists of a nearly equilaterally shaped triangular protonic frame with two electrons in the  $1sa_1$  state ( $D_{3h}$  symmetry, when neglecting the Jahn-Teller effect). The third electron orbits around that core and transitions between states of this valence electron are responsible for the observed spectra.

Apparently only the neutralized ion-beam method is suitable to measure the rather weak uv spectra of the isotopomers of triatomic hydrogen. Since the isotopomers can be mass selected, it is possible to suppress uv spectra of other species such as  $H_2$ . However, there is one exception:  $H_2D^+$  cannot be separated from  $D_2^+$  also present in the ion beam since both ions have equal charge-to-mass ratios. Therefore, the stronger  $D_2$  radiation is blended into the  $H_2D$  spectra, in particular in the uv.

Raksit *et al.* investigated the spectra of  $D_3$  in the uv region [7]. Their detection system seems to have been sensitive only below 300 nm and they apparently missed a part of the uv spectrum. They found a continuum peaked at about 300 nm.

Contrary to that, in the work reported here, the continuum shows two distinct broad maxima at about 240 and 310 nm. These maxima could be attributed to the Jahn-Teller structure of the ground-state potential surface that has two energetically clearly separated sheets [8]. This interpretation of the bimodal structure of the uv spectra is supported here by numerical simulations of the spectra incorporating *ab initio* transition moments and potential surfaces. In addition, lifetimes on both sheets of the Jahn-Teller ground-state surface are derived from the simulation of the uv spectra.

\*Present address: Institut für Laserphysik, Jungiusstrasse 9, 20355 Hamburg, Germany.

†Author to whom correspondence should be addressed.

We also present in this article measurements of radiative lifetimes of the  $n=3$  Rydberg states that have been identified as the emitters of the uv radiation. These lifetimes have been determined from the exponential decay of the light intensity after neutralization along the molecular beam.

The organization of the remainder of this article is as follows. In Sec. II the experimental technique and procedures necessary for the measurement of lifetimes and uv spectra are summarized. Section III is concerned with the interpretation of the lifetime measurements of the uv emitting Rydberg states with principal quantum number  $n=3$ . In Sec. IV the numerical simulation of the uv spectra is described. Section IV A outlines the *ab initio* calculations of electric-dipole transition moments between  $n=3$  Rydberg states and the electronic ground state of  $H_3$  and in Sec. IV B the calculation of the uv spectra is described. Then a discussion of the lifetimes on the ground-state surface extracted from the numerical simulations of the uv spectra follows in Sec. V. Finally, some concluding remarks in Sec. VI complete the article.

## II. EXPERIMENT

The ion-beam neutralization apparatus has been used for many previous studies and is described in detail in earlier publications (e.g., [9,10]). Therefore, after describing the main features of the apparatus, only details specific for this experiment will be given.

The molecular ions  $H_3^+$ ,  $H_2D^+$ ,  $D_2H^+$ , and  $D_3^+$  with mass numbers 3, 4, 5, and 6, respectively, are formed in a duoplasmatron, which in essence is a hollow cathodelike dc discharge run through the relevant gases, in this case through hydrogen or deuterium or a mixture of both with the ratios 2:1 and 1:2, respectively. Ions are extracted through a hole in the anode and accelerated by a high voltage (15 keV). The ion beam is focused using an Einzel lens and directed to a sector magnetic field by crossed condenser fields. After passing through another electrostatic lens, the mass-selected beam traverses a cesium vapor cell for neutralization. Since an electron is captured into excited states of the neutralized molecules, photon emission arising from radiative decay to the ground state can be observed inside and behind the cesium cell. This light is focused by several mirrors to a spectrograph (3-m monochromator), spectrally resolved and then detected by a photon multiplier (RCA Model No. C 31034).

### A. Lifetime measurements

After traversal of the charge exchange cell, the light intensity decreases exponentially along the neutralized molecular beam. A practical way to measure that decay as a function of the distance along the beam is to image a small part of the radiating molecular beam to the entrance slit of the monochromator and move the neutralization cell relative to the point of observation. Since the velocity of the molecules is known, the light intensity of a given molecular spectral line can be measured as a function of time. Thus, for example, the lifetimes of single rovibrational levels can be deduced [9–11].

About ten different wavelengths of the uv continua of every isotopomer were selected and the lifetimes measured at these wavelengths. By comparison with the lifetimes ob-

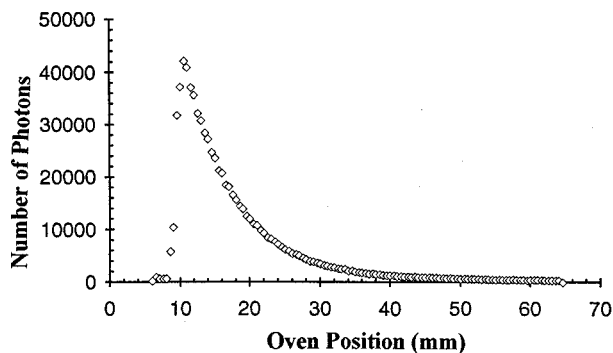


FIG. 1. Typical lifetime measurement. Dividing the oven position by the velocity of the molecules yields the time axis.

tained from discrete spectra in the visible, the uv lifetimes then served to identify the upper levels responsible for the uv emission: the  $n=3$  Rydberg states.

The lifetimes of the  $n=3$  uv emitting levels have been measured as follows. A computer-controlled stepper motor moved the cesium oven along the beam line in 1-mm steps. At each step the emitted number of photons was counted for 10 s. The ion-beam current was between 20 and 40  $\mu A$  and the beam had a diameter of 2 mm. For normalization, the fraction of the ion beam not neutralized in the charge exchange cell was measured using a Faraday cup as a function of the oven position. To extract lifetimes from data as shown in Fig. 1, a linear combination  $A(t)$  of exponential functions was fitted to the experimental data (after subtraction of the dark counts of the photomultiplier). Two exponentials with four variable parameters were sufficient to reach a good fit:

$$A(t) = A_1 e^{-t/t_1} + A_2 e^{-t/t_2}, \quad (1)$$

where the first term on the right-hand side decays appreciably faster than the second one ( $t_1 < t_2$ ) and mainly describes the effect of the uv radiation that is investigated here. Two physical origins of the second term with amplitude  $A_2$  are conceivable. (i) There is cascading from higher levels with  $n > 3$ . However, this should not play an appreciable role because transition probabilities between higher Rydberg states and the  $n=3$  levels are relatively small. (ii) Since cesium atoms can escape from the neutralization cell in the direction of the ion beam, neutralization can also take place outside the cesium cell. Therefore, a new population of the  $n=3$  levels in the region observed by the light detection system can be created. In Table I the results of the fit procedure are listed for the molecule  $D_3$ . The relative amplitude  $A_1$  of the first term that describes the lifetime of the uv emitting states is much larger than  $A_2$  (we have  $A_1 + A_2 = 1$ ).

For these measurements mixtures of  $H_2$  and  $D_2$  were prepared in stainless-steel containers connected to the duoplasmatron where a pressure of about 140 Pa was maintained. The slit widths of the monochromator was varied between 0.5 and 1 mm, which corresponded to a spectral resolution of 0.5–1 nm. The maximal count rates were 290 counts per second (cps) for  $H_3$ , 700 cps for  $D_3$ , 150 cps for  $D_2H$ , and 225 cps for  $H_2D$ .

The  $H_2D^+$  and  $H_3^+$  ion beams were disturbed by ions with the same masses, i.e.,  $D_2^+$  and  $HD^+$ , respectively. De-

TABLE I. Two lifetimes are extracted from double-exponential fits [Eq. (1)] to the experimental data for  $D_3$  at 11 different wavelengths (compare Fig. 1). The relative amplitude  $1 - A_1$  of the longer decay time  $t_2$  is only a few percent of that of the short decay time  $t_1$ . In the last row the weighted average lifetimes  $\bar{t}_{1,2}$  are given.

Wavelength (nm)	$t_1$ (ns)	$A_1$ at $x=10$ mm	$t_2$ (ns)
203.5	$10.7 \pm 0.5$	0.99	
222.5	$10.3 \pm 0.3$	0.97	$27 \pm 7$
244.0	$10.2 \pm 0.2$	0.96	$26 \pm 4$
266.2	$10.1 \pm 0.3$	0.94	$25 \pm 4$
289.7	$9.9 \pm 0.2$	0.95	$26 \pm 2$
309.0	$9.8 \pm 0.1$	0.95	$28 \pm 2$
328.4	$9.5 \pm 0.2$	0.93	$23 \pm 2$
328.4	$9.5 \pm 0.3$	0.93	$24 \pm 3$
348.1	$10.1 \pm 0.2$	0.97	$32 \pm 9$
370.3	$9.3 \pm 0.3$	0.92	$27 \pm 4$
392.5	$10.2 \pm 0.4$	0.87	$33 \pm 5$
Weighted average	$\bar{t}_1 = 9.9 \pm 0.4$	0.94	$\bar{t}_2 = 26 \pm 4$

spite that, the lifetimes of interest could be approximately determined by measuring the lifetimes of  $D_2$  separately (29.1 ns) using very pure gases and different ion sources for different isotopomers.

### B. Measurement of the uv spectra

The knowledge of the spectral response of the whole detection system (imaging mirrors, monochromator, and photomultiplier tube), i.e., the detection sensitivity as a function of wavelength in the relevant range 180–450 nm, was particularly important in order to obtain correct spectra. Deuterium lamps (made by Oriel and Hamamatsu) whose spectral distributions are known were employed for calibration purposes and, in addition, the blackbody radiation of a tungsten ribbon at different temperatures was used. Finally, the mean spectral response obtained from these different sources was used to correct the measured molecular spectra. An accuracy of 5–10% is estimated for the final calibration curve in Fig. 2.

The same calibration curve was used in earlier work for the correction of ArH and ArD uv spectra [12], which were consistent with theory and also other experimentalists' results. This served as an important check for the validity of this calibration curve.

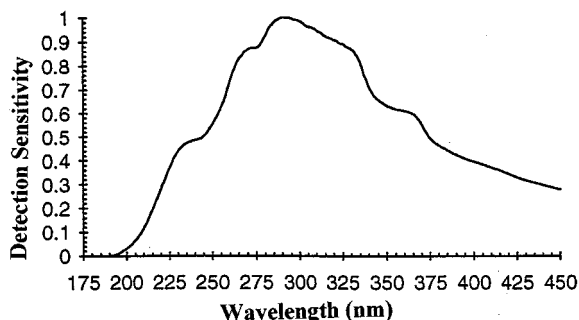


FIG. 2. Normalized spectral response of the combined light detection system (imaging optics, monochromator, and photomultiplier).

Figure 3 demonstrates the very good reproducibility of the  $D_3$  uv spectrum (corrected for the spectral response) that was obtained after optimization of the charge exchange system and the ion-beam stability. Discrete lines on the smooth curve have been identified as cesium atomic lines and have been removed by a suitable procedure before interpreting the uv spectra. The corrected uv spectra of all four isotopomers are shown in Figs. 4(a)–4(d).

Varying the gas pressure in the ion source (leading potentially to different population probabilities for rovibrational levels) did not have a marked influence on the shape of the  $D_3$  spectrum as can be seen in Fig. 5. During extraction from the duoplasmatron, vibrational excitation of molecular ions is quenched in collisions with neutral gas escaping from the ion source. This relaxation mechanism is more effective for higher gas pressure in the ion source. Thus, by varying the pressure one has some control over the vibrational excitation of the molecular ions. Only after reducing the pressure by a factor 7, from 150 to 23 Pa, a slight broadening of the uv spectrum has been observed (Fig. 5, the three spectra are normalized to have the same emission intensity at 300 nm), which indicates a contribution to the spectrum from excited vibrational  $n=3$  states.

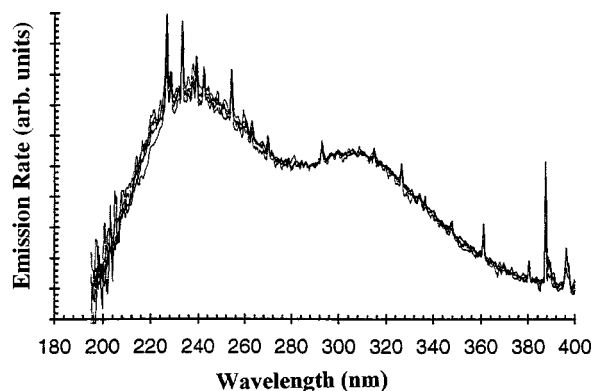


FIG. 3. Reproducibility of the measurements of the  $D_3$  spectrum. Five measurements are shown here, recorded one after the other without changing any instrumental parameter, each of them corrected using the curve in Fig. 2.

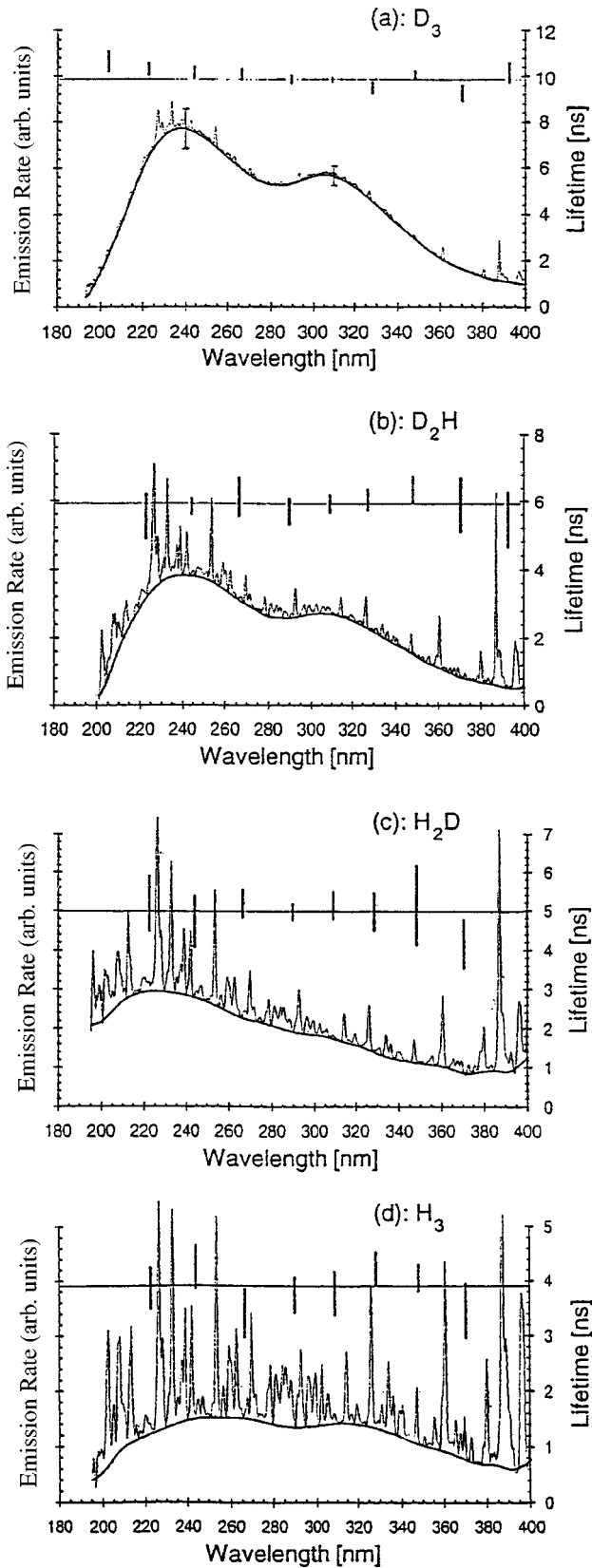


FIG. 4. uv spectra of all isotopomers corrected for the detection sensitivity. The ordinate on the right-hand side indicates the measured lifetimes as a function of wavelength. The  $\text{H}_2\text{D}$  spectrum is strongly disturbed by  $\text{D}_2$  emission around 220 nm and therefore does not exhibit the typical bimodal structure.

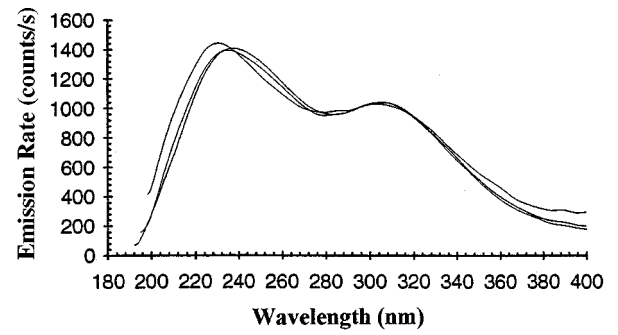


FIG. 5.  $\text{D}_3$  spectrum recorded with different pressures in the ion source. For 150 and 72 Pa the normalized spectra nearly coincide. The spectrum at 23 Pa shows a slightly different intensity at short and long wavelengths. The count rates before normalization at 300 nm are 3800, 2150, and 470 counts per second, respectively.

The overall intensity of uv emission depended strongly on the ion source pressure. Changing the pressure *inside* the ion source leads to different plasma dynamics, which in turn influences the electronic excitation of the ions. This leads to different charge-exchange cross sections [13] for the  $n=3$  states and thus to different intensities in the uv spectra. All the spectra shown in this article (except Fig. 5) were taken at pressures between 100 and 150 Pa with the molecules in their vibrational ground state.

### III. LIFETIME MEASUREMENTS OF THE $n=3$ STATES IN THE UV

In addition to the spectra, the results of lifetime measurements are also indicated in Fig. 4. We find only a rather small variation with no systematic trend in the lifetimes measured in the uv range between 200 and 400 nm as a function of wavelength. Therefore, it makes sense to determine an average value of these lifetimes characteristic for each isotopomer, as is shown in Table II.

The lifetimes  $t_1$  in Table II show a characteristic decrease from  $\text{D}_3$  over  $\text{D}_2\text{H}$  and  $\text{H}_2\text{D}$  to  $\text{H}_3$  from 9.87 to 3.91 ns. It is important to note that the lifetimes of the  $n=3$  levels deduced from visible light emission showed the same behavior (Table III). Furthermore, the radiation intensity in the uv for the different isotopomers decreases also in this order (Fig. 4). This is attributed to the fact that predissociation, as the

TABLE II. The weighted average values of the short lifetime component  $\bar{t}_{1,2}$  for all isotopomers are reported. The third column displays the relative amplitude of the short lifetime component  $A_1$ .  $\text{H}_2\text{D}$  has a much larger component with a long lifetime, namely, with about 40%. This might be due to the admixture of the molecule  $\text{D}_2$  in the neutralized beam. In the fifth row also a lifetime for  $\text{D}_2$  is reported that was measured in the same wavelength range.

Molecule	$\bar{t}_1$ (ns)	$A_1$	$\bar{t}_2$ (ns)
$\text{D}_3$	$9.9 \pm 0.4$	0.94	$26 \pm 4$
$\text{D}_2\text{H}$	$5.9 \pm 0.4$	0.83	$12 \pm 5$
$\text{H}_2\text{D}$	$5.0 \pm 0.5$	0.61	$31 \pm 2$
$\text{H}_3$	$3.9 \pm 0.5$	0.81	$21 \pm 6$
$\text{D}_2$	$29.1 \pm 1.5$		

TABLE III. Lifetimes measured here in the uv (last row) are compared with those measured previously for the same  $n=3$  levels in the visible spectra (rows 1–4) [9,10].

State	D <sub>3</sub>	D <sub>2</sub> H	H <sub>2</sub> D	H <sub>3</sub>
$3d\ ^2A'_1$				
$3d\ ^2E''$	11.4–12.2	7.5–9.3	5.6–8.7	3.5–11.0
$3d\ ^2E'$				
$3p\ ^2A''_2$		7.8–15	7.5–29	4.1–35
$3s\ ^2A'_1$	9.7–12.5	5.2	4.1	
$3p\ ^2E'$	$17.5 \pm 2$	$5 \pm 0.7$	$2.5^{+0.3}_{-0.7}$	$1.1^{+0.2}_{-1}$
uv	$9.9 \pm 0.4$	$5.9 \pm 0.5$	$5.0 \pm 0.5$	$3.9 \pm 0.5$

competing effect to radiative decay, increases for the  $n=3$  levels in this isotopomer series. This was observed in the visible spectra of these isotopomers, namely, in the 5600-, 5800-, 6012-, and 7100-Å bands [1,4,5].

A qualitative explanation for these observations might give the tunnel effect: The lighter H atoms escape faster through the bonding potential barrier than D atoms. This was also observed for other isotopic molecules such as OH and OD or rare-gas hydrides.

In addition to the aspects discussed above, the lifetimes measured here allow us to determine the emitters of the uv radiation. Considering the wavelength range of the uv radiation only, it must be concluded that the  $n=3$  Rydberg states are the emitters. The lifetime measurements give more details: In Table III the lifetimes measured in the uv are compared to the lifetimes of the electronic  $n=3$  levels deduced from light emission in the visible spectrum [9,10], where the states can be resolved according to orbital angular momentum and group-theoretical assignment ( $D_{3h}$  and  $C_{2v}$  groups). We find that the uv lifetimes are closest to those in the visible spectrum of the  $3s$  and  $3d$  states and differ appreciably from that of the  $3p\ ^2E'$  state. This suggests that the main contributors to the uv radiation are the  $3s$  and  $3d$  states, as it is expected from the transition rules for the simple Rydberg model invoked for these molecules. Apparently, there are also exceptions to this statement, as is seen from Table III. The discussion of these exceptions are beyond the scope of this article and will not be considered here.

#### IV. SIMULATION OF THE UV SPECTRA

The transitions responsible for uv emission terminate on the ground state and it will be shown in what follows that the characteristic shape of the uv spectra is due to the structure of this ground-state potential surface. The ground-state surface of triatomic hydrogen was extensively studied by *ab initio* calculations by Eyring and Polanyi [14], Siegbahn and Liu [15], Truhlar and Horowitz [16], and Porter and Karplus [17]. In particular the work of Porter and Karplus and illustrations therein, impressively show the main features of the ground-state surface of H<sub>3</sub>, e.g., its Jahn-Teller character. Here we want to consider that part of the potential surface that is a function of the asymmetric vibrational coordinates  $q_1$  and  $q_2$ . These coordinates describe the deviation of the three protons from  $D_{3h}$  symmetry (equilateral triangle). The symmetric stretch displacement  $q_0$  from an equilateral tri-

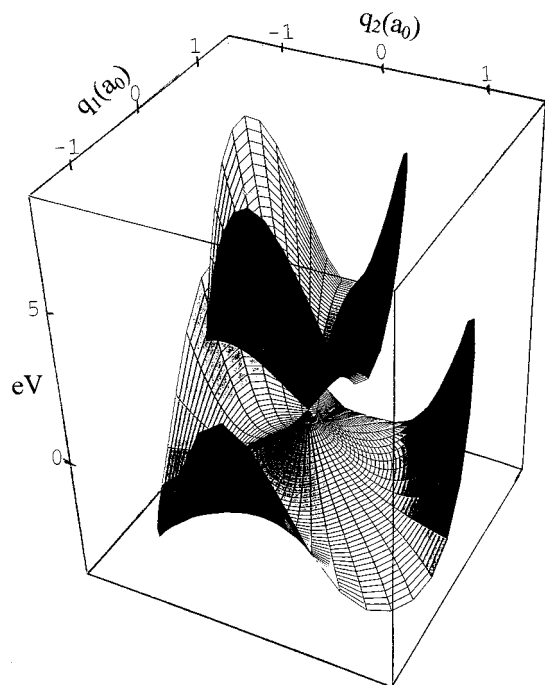


FIG. 6. That part of the H<sub>3</sub> ground-state surface on which the asymmetric vibration of the nuclei takes place (described by vibrational coordinates  $q_1$  and  $q_2$ ). The Jahn-Teller structure of H<sub>3</sub> can be seen: a lower and an upper sheet and the cone for  $q_1=q_2=0$ . At the origin the molecule takes on  $D_{3h}$  symmetry, otherwise  $C_s$  symmetry.

angle with side  $R_0=1.65a_0$  (equilibrium geometry for the Rydberg states and the cation H<sub>3</sub><sup>+</sup>; cf. the work of Porter, Stevens, and Karplus [17]) describes the symmetric “breathing” mode of vibration. The inner part of the potential surface consists of an upper bonding sheet connected by a cone to a partly dissociative lower sheet exhibiting three characteristic “saddles” (Fig. 6). In alkali trimers, for example, the “lower” sheet has, like the “upper” one, also bonding character, which leads to a splitting of the bound vibrational energy levels in these molecules [18]. The dissociative character of the lower sheet of the H<sub>3</sub> ground-state surface implies a large energetic separation between the two sheets, which can easily be observed spectroscopically. These features can be described by an analytic expression [17,19]

$$E_{\pm} = E(q=0) + A \pm B, \quad (2)$$

with

$$A = 0.1011q^2 - 0.0989q^3 \cos 3\varphi + \dots$$

and

$$B = 0.12168q - 0.0256q^2 \cos 3\varphi \\ + (0.0235 \cos^2 3\varphi)q^3 + \dots$$

This two signs refer to the two sheets that intersect at the point  $q=0$ . The polar coordinates  $q$  and  $\varphi$  are defined by  $q_1 = q \cos \varphi$  and  $q_2 = q \sin \varphi$ .

The ground-state surface as a function of the asymmetrical coordinates  $q_1$  and  $q_2$  according to Eq. (2) is plotted in

TABLE IV. Calculated energies (hartree) of the ground and  $n=3$  states of  $H_3$  for different values of  $q$  ( $a_0$ ) and  $\varphi$ . The side length of the equilateral triangle is  $q_0+R_0=1.65a_0$ .

State	$q=0$	$q=0.25,$ $\varphi=0^\circ$	$q=0.5,$ $\varphi=0^\circ$	$q=0.25,$ $\varphi=180^\circ$	$q=0.5,$ $\varphi=180^\circ$	$q=0.25,$ $\varphi=90^\circ$	$q=0.5,$ $\varphi=90^\circ$
$1^2A'(2p)$	-1.555 611	-1.581 489	-1.597 342	-1.581 482	-1.581 272	-1.581 531	-1.590 534
$2^2A'(2p)$	-1.555 613	-1.519 705	-1.483 169	-1.513 606	-1.444 873	-1.516 622	-1.464 676
$4^2A'(3p)$	-1.412 108	-1.408 037	-1.393 918	-1.405 059	-1.365 300	-1.406 570	-1.380 607
$5^2A'(3p)$	-1.412 108	-1.400 704	-1.380 712	-1.396 685	-1.348 309	-1.398 698	-1.365 361
$6^2A'(3s)$	-1.397 368	-1.389 483	-1.372 028	-1.385 980	-1.341 434	-1.387 744	-1.357 660
$7^2A'(3d)$	-1.394 869	-1.387 381	-1.370 875	-1.383 714	-1.340 151	-1.385 609	-1.356 434
$8^2A'(3d)$	-1.394 868	-1.387 190	-1.370 273	-1.383 839	-1.339 671	-1.385 482	-1.355 916
$9^2A'(3d)$	-1.392 836	-1.385 055	-1.367 891	-1.381 566	-1.337 364	-1.383 324	-1.353 558
$2^2A''(3p)$	-1.396 195	-1.388 458	-1.371 330	-1.384 961	-1.340 786	-1.386 726	-1.356 992
$3^2A''(3d)$	-1.393 186	-1.385 845	-1.369 252	-1.382 321	-1.338 539	-1.384 060	-1.354 828
$4^2A''(3d)$	-1.393 185	-1.385 185	-1.367 931	-1.381 708	-1.337 439	-1.383 492	-1.353 612

TABLE V. Dipole transition moments (a.u.) between  $n=3$  Rydberg states of  $H_3$  and the  $1^2A'$  and  $2^2A''(2p)$  states at different values of the polar coordinates  $q$  ( $a_0$ ) and  $\varphi$ ;  $q_0+R_0=1.65a_0$ . The appropriate component of the transition moment is given in the second row.

Transition		$q=0$	$q=0.25,$ $\varphi=0^\circ$	$q=0.5,$ $\varphi=0^\circ$	$q=0.25,$ $\varphi=180^\circ$	$q=0.5,$ $\varphi=180^\circ$	$q=0.25,$ $\varphi=90^\circ$	$q=0.5,$ $\varphi=90^\circ$
$4^2A' \rightarrow 1^2A'$	$x$	0.0	0.0	0.0	0.0	0.0	0.031 88	0.108 70
	$y$	0.090 98	0.373 17	0.011 40	0.078 51	0.166 07	0.049 27	0.054 93
$4^2A' \rightarrow 2^2A'$	$x$	0.090 75	0.219 87	0.767 31	0.071 82	0.091 32	0.164 16	0.555 97
	$y$	0.0	0.0	0.0	0.0	0.0	0.046 04	0.184 43
$5^2A' \rightarrow 1^2A'$	$x$	0.090 15	0.151 20	0.240 74	0.195 76	0.171 79	0.0	0.084 65
	$y$	0.0	0.0	0.0	0.0	0.0	0.177 98	0.201 58
$5^2A' \rightarrow 2^2A'$	$x$	0.0	0.0	0.0	0.0	0.0	0.267 70	0.480 28
	$y$	0.090 38	0.386 01	0.802 68	0.195 65	0.375 62	0.139 60	0.413 49
$6^2A' \rightarrow 1^2A'$	$x$	0.206 73	0.272 22	0.262 70	0.0	0.0	0.247 57	0.301 85
	$y$	0.0	0.0	0.0	0.304 45	0.347 73	0.164 48	0.126 47
$6^2A' \rightarrow 2^2A'$	$x$	0.0	0.0	0.0	0.078 04	0.203 04	0.073 35	0.056 92
	$y$	0.248 80	0.134 15	0.141 23	0.0	0.0	0.073 36	0.090 58
$7^2A' \rightarrow 1^2A'$	$x$	0.0	0.649 56	0.538 71	0.580 26	0.0	0.303 15	0.440 03
	$y$	0.772 02	0.0	0.0	0.0	0.445 03	0.545 62	0.184 87
$7^2A' \rightarrow 2^2A'$	$x$	0.772 01	0.0	0.0	0.0	1.000 51	0.819 23	0.383 56
	$y$	0.0	0.842 97	0.807 25	1.014 58	0.0	0.351 79	0.842 10
$8^2A' \rightarrow 1^2A'$	$x$	0.775 32	0.0	0.0	0.0	0.436 55	0.534 96	0.166 49
	$y$	0.0	0.600 45	0.488 17	0.616 30	0.0	0.264 55	0.428 66
$8^2A' \rightarrow 2^2A'$	$x$	0.0	0.981 52	1.142 65	0.899 54	0.0	0.476 64	1.065 59
	$y$	0.767 89	0.0	0.0	0.0	1.297 19	0.856 91	0.594 29
$9^2A' \rightarrow 1^2A'$	$x$	0.381 03	0.163 87	0.056 91	0.0	0.0	0.134 67	0.060 73
	$y$	0.0	0.0	0.0	0.163 53	0.056 42	0.084 07	0.014 65
$9^2A' \rightarrow 2^2A'$	$x$	0.0	0.0	0.0	0.696 21	1.086 73	0.409 58	0.468 80
	$y$	0.370 90	0.680 22	0.924 00	0.0	0.0	0.556 30	0.876 37
$2^2A'' \rightarrow 1^2A'$	$z$	0.0	0.0	0.0	0.038 95	0.043 93	0.028 20	0.035 61
$2^2A'' \rightarrow 2^2A'$	$z$	0.010 00	0.107 32	0.324 74	0.0	0.0	0.075 91	0.234 78
$3^2A'' \rightarrow 1^2A'$	$z$	0.0	0.550 07	0.451 51	0.529 77	0.397 96	0.533 55	0.421 40
$3^2A'' \rightarrow 2^2A'$	$z$	0.707 03	0.0	0.0	0.0	0.0	0.124 95	0.142 24
$4^2A'' \rightarrow 1^2A'$	$z$	0.707 05	0.0	0.0	0.0	0.0	0.081 73	0.022 61
$4^2A'' \rightarrow 2^2A'$	$z$	0.0	0.899 41	1.036 91	0.940 83	1.240 54	0.911 93	1.133 06

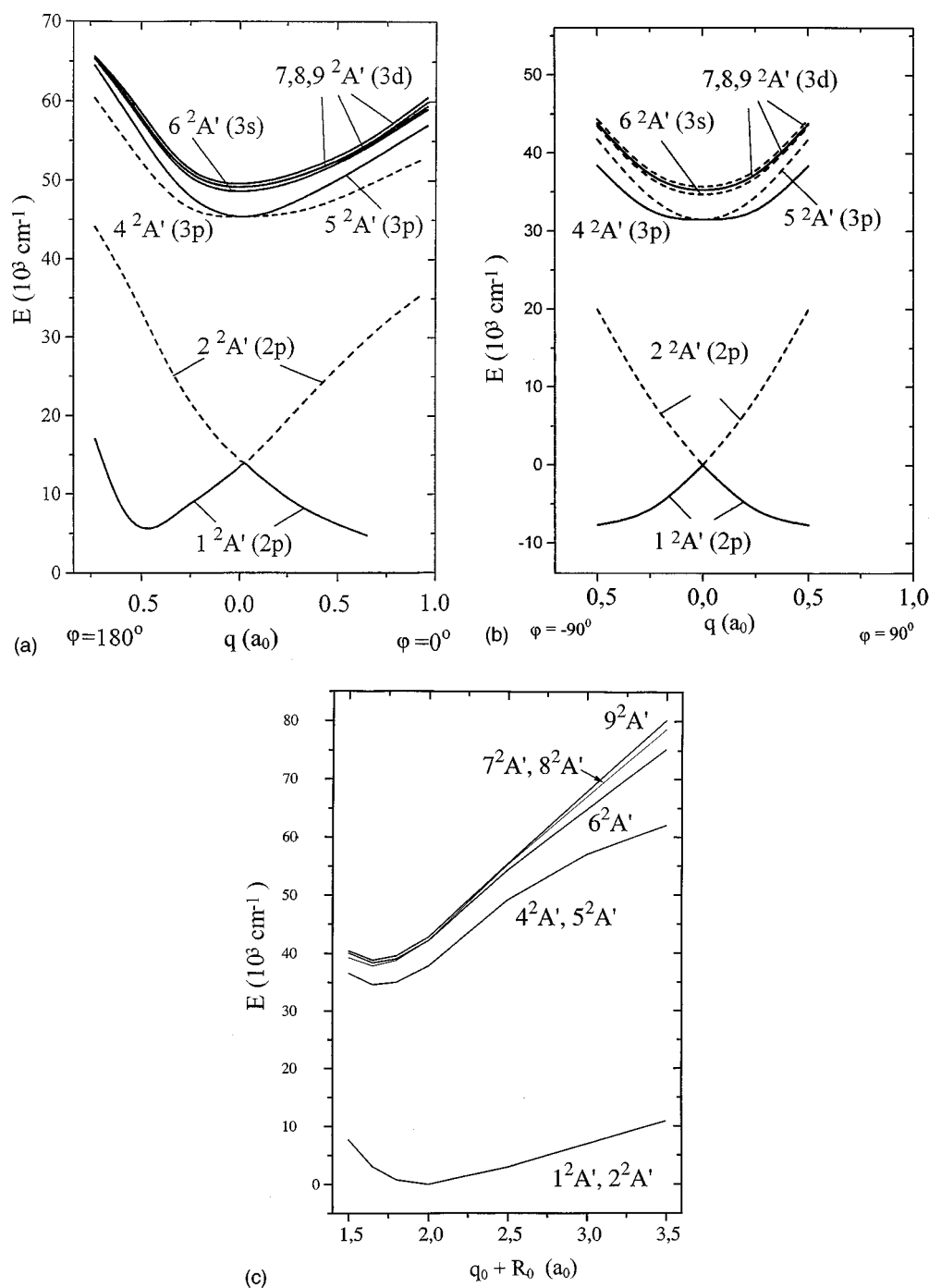


FIG. 7. (a) Potential energies calculated *ab initio* as a function of  $q, \varphi = 0, \pi$ , i.e., as a function of the asymmetric vibrational coordinate  $q_1$ . The potentials labeled  $1^2A'$  and  $2^2A'$  represent the lower and upper parts, respectively, of the ground state, while  $4^2A'$  to  $9^2A'$  are the excited states  $3s$ ,  $3p$ , and  $3d$ . Designations of the states are given in  $C_s$  symmetry. The curves belong to the equilibrium side length  $q_0 + R_0 = 1.65a_0$ . (b) Potential-energy curves as a function of  $q, \varphi = \pm \pi/2$ , i.e., as a function of the asymmetric vibrational coordinate  $q_2$ ;  $q_0 + R_0 = 1.65a_0$ . (c) Potential-energy curves as a function of the side length  $q_0 + R_0$  of the equilateral triangle.

Fig. 6. It is interesting to note that the part of the potential surface that is a function of the symmetric coordinate  $q_0$  is bonding, as can be seen in Fig. 7(c) [e.g., [20]].

The shape of the ground-state surface suggests that the two maxima of the uv spectra are due to the decay of the  $n = 3$  Rydberg states into the two sheets of this surface: The observed energy separation of the two maxima in the uv spectra of about  $9600 \text{ cm}^{-1}$  is approximately equal to the energy gap between the upper and lower sheets of the

ground-state surface [8]. The continuous spectra, in which individual rovibronic transitions are not resolved, point to a very short lifetime on both sheets, which should be in the femtosecond range.

In one approach the spectrum of  $D_3$  was simulated using linear two-dimensional approximations to the ground-state potential. For the transition moments a linear expression in the coordinates  $q_0, q_1$ , and  $q_2$ , was assumed, which contained two fit parameters. A satisfactory fit was obtained

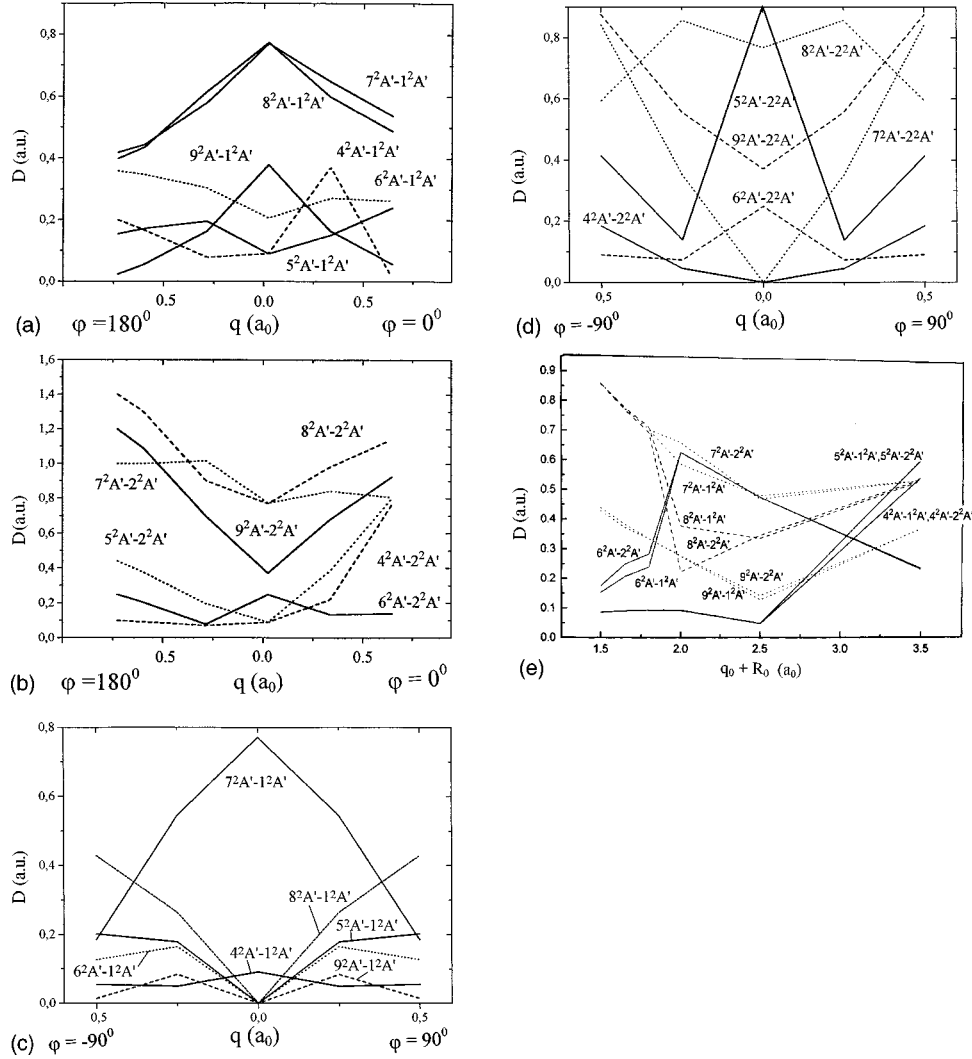


FIG. 8. Electric-dipole transition moments  $D_{e'e''}(q) = |\langle \Psi_{e'}(q) | d | \Psi_{e''}(q) \rangle|$  as a function of  $q, \varphi = 0, \pi$  between  $n=3$  states ( $4^2A' - 9^2A'$ ) and (a) the lower and (b) the upper sheet of the ground state;  $q_0 + R_0 = 1.65a_0$ . Electric-dipole transition moments as a function of  $q$  for the cross section  $\varphi = \pm \pi/2$  between  $n=3$  states and (c) the lower and the (d) upper sheet of the ground state;  $q_0 + R_0 = 1.65a_0$ . (e) Dipole transition moments as a function of the side length  $q_0 + R_0$  of the equilateral triangle.

only for  $D_3$ . It supported strongly the interpretation of the bimodal uv spectra as being due to radiative decay into the two sheets of the ground-state surface [8]. In this work the spectra of  $D_3$ ,  $D_2H$ , and  $H_3$  are simulated by making full use of *ab initio* potential curves and electric-dipole transition moments.

#### A. *Ab initio* calculations of the potential-energy surfaces and the transition moments

Theoretical *ab initio* calculations have been carried out on the electronic states of  $H_3$ , extending our previous calculations to geometries required for the purposes of the present work [20]. The atomic-orbital basis employed is identical to that of the previous work. The molecular geometries were generated to lie in the region  $0.0a_0 \leq q \leq 0.5a_0$ ,  $1.5a_0 \leq R_0 \leq 3.5a_0$ , and  $0 \leq \varphi \leq 2\pi$ , where  $q_0$  is the symmetric stretch displacement from an equilateral triangle with side  $R_0$  (equilibrium geometry for the Rydberg states and the cation  $H_3^+$ ); cf. Ref. [17]. The sides of the triangle  $R_1$ ,  $R_2$ , and  $R_3$  are related to  $q_0$ ,  $q$ , and  $\varphi$  [17] by

$$\begin{aligned}
 R_1 &= [(R_0 + q_0)^2 + q^2 - (R_0 + q_0)q \cos \varphi \\
 &\quad - \sqrt{3}(R_0 + q_0)q \sin \varphi]^{1/2}, \\
 R_2 &= [(R_0 + q_0)^2 + q^2 - (R_0 + q_0)q \cos \varphi \\
 &\quad + \sqrt{3}(R_0 + q_0)q \sin \varphi]^{1/2}, \\
 R_3 &= [(R_0 + q_0)^2 + q^2 + 2(R_0 + q_0)q \cos \varphi]^{1/2}.
 \end{aligned} \tag{3}$$

All present calculations have been carried out in  $C_s$  symmetry, which is common to all the different geometries. The multireference double configuration-interaction (MRDCI) method and programs [21] were employed for the calculations. Nine states of  $^2A'$  and five  $^2A''$  states have been calculated, which correspond to the ground and excited states of  $H_3$  up to  $(3d)$   $^2A'$  and up to the  $(4p)$   $^2A''$  states (cf. [20]). Configuration-interaction spaces of 35 442 and 25 726 configurations functions, respectively, were generated by all single and double substitutions from reference spaces of 91 and 47 configurations for the  $^2A'$  and the  $^2A''$  calculations, respectively. The present calculations involved all the gener-

ated configurations, without any selection. The results of the calculations, in terms of energies and dipole transition moments, at 50 different molecular geometries may be obtained directly from the authors. In Table IV the calculated energies of the ground and the  $n=3$  Rydberg states for  $R_0=1.65a_0$  ( $q_0=0$ ) are listed, while the corresponding dipole transition moments are listed in Table V. Some cuts through the potential-energy surfaces and the dipole transition moment surfaces have been plotted in Figs. 7 and 8. Considering the molecules to be rotating, the potentials were supplemented by a bonding part proportional to  $j''(j''+1)$  [22].

### B. Calculation of the uv spectra and their interpretation

First, the intensity of each rovibronic transition has been calculated and then the contributions from each line were summed to obtain the continuous total uv spectrum. The emission intensity  $I$  due to a transition from an  $n=3$  rovibronic state  $|e',v',j'\rangle$  to a lower discrete rovibronic state  $|e'',v'',j''\rangle$  is given by [22]

$$I_{e'e''v'v''j'j''} = \frac{64}{3} \pi^4 c f^4 g N(v',j') \times \frac{S_{j'j''}}{2j'+1} | \langle v',j' | D_{e'e''}(q) | v'',j'' \rangle |^2. \quad (4)$$

Here  $e$  symbolizes the electronic quantum numbers,  $v$  the vibrational, and  $j$  the total angular momentum quantum number.  $N(v',j') = N_0(2j'+1)e^{-E(v',j')/KT}$  is the Boltzmann population of the upper level, with  $N_0$  being a normalization constant,  $k$  the Boltzmann constant, and  $T$  the absolute temperature.  $S_{j'j''}$  stands for the rotational transition matrix element (the Hönl-London factor) and  $D_{e'e''}(q) = \langle \Psi_{e'}(q) | d | \Psi_{e''}(q) \rangle$ , with  $d$  being the dipole operator.

The coordinate  $q$  describes the amount of distortion of the equilateral triangle, whereas  $\varphi$  indicates the ‘‘direction’’ of this distortion in the  $q_1$ - $q_2$  plane ( $q_1 = q \cos \varphi$  and  $q_2 = q \sin \varphi$ ). The *ab initio* calculated electronic transition matrix elements  $D_{e'e''}$  as a function of the nuclear coordinate  $q$  are shown in Fig. 8.  $f = (E_{e'} - E_{e''})/hc$ , is the transition frequency,  $E_{e'}, E_{e''}$  being the electronic term values. Finally,  $g = (2 - \delta_{0,\Lambda'+\Lambda''}) / (2 - \delta_{0,\Lambda'})$  is the degeneracy factor, where  $\Lambda$  is the projection of the electronic orbital angular momentum on the molecular axis. The  $A$  states have  $\Sigma$  character; consequently,  $\Lambda' = \Lambda'' = 0$ , yielding  $g = 1$ . The vibrational wave functions have been calculated by numerically solving the Schrödinger equation (Numerov-Cooley method [23]) using *ab initio* potentials of the upper and lower states [20]. Some of the potentials used in this simulation have been determined previously [20]. Others (see Fig. 7) have been calculated specifically for this work.

If the lower molecular state is a continuum in the nuclear coordinates, Eq. (4) has to be modified:  $|v'',j''\rangle$  has to be replaced by  $|E'',j''\rangle$  and one has to integrate  $E''$  over the possible energy range  $\Delta E$  of the continuum states. In this case, the appropriate expression for the emission intensity  $I(\lambda)$ .  $\lambda = c/f$  is the emission wavelength is

$$I(\lambda)_{e'e''v'v''j'j''} = \frac{64}{3} \pi^4 c^2 f^6 g N(v',j')$$

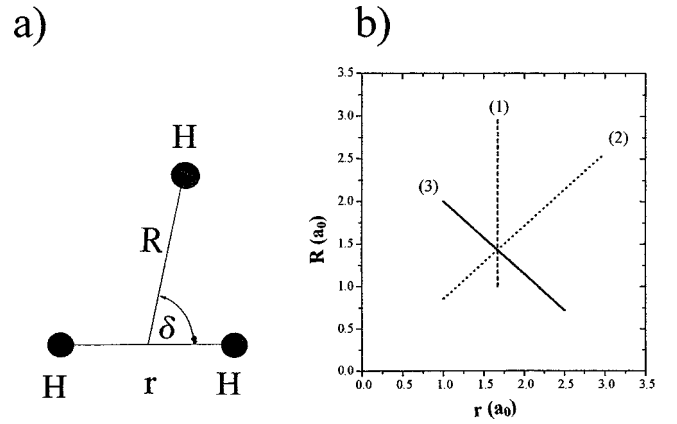


FIG. 9. (a) Definition of the Jacobi coordinates  $R, r, \delta$  (b) Different relative motions of the nuclei in  $H_3$ : the reaction trajectory (1), the symmetric vibrational motion (2) (described by the normal coordinate  $q_0$ ), and the degenerate asymmetric vibrational motion (3), which can be described by normal coordinates  $q_1$  and  $q_2$ . The  $q_1$  vibration is described by (3) while the vibration  $q_2$  lies outside the  $R$ - $r$  plane. The end points of the straight lines indicate the ranges for which potential curves and transition dipole moments have been calculated *ab initio*.  $Q_2$  was varied in the interval  $[-0.5a_0 \leq q_2 \leq 0.5a_0]$  (compare Figs. 7 and 8 and Tables IV and V).

$$\times \frac{S_{j'j''}}{2j'+1} | \langle e',v',j' | D_{e'e''}(q) | E'',j'' \rangle |^2. \quad (5)$$

In order to carry out the numerical calculation of vibrational wave functions, the vibrational motion of the nuclei has been separated into the symmetric breathing mode (dependent only on  $q_0$ ) and the asymmetric vibration dependent on  $q$  and  $\varphi$ . Individual rovibronic transitions have been calculated for the symmetric vibrational mode with  $R_0 + q_0$  varying between  $1.5a_0$  and  $3.5a_0$  [see Fig. 7(c);  $a_0$  stands for the Bohr radius and  $R_0$  is the equilibrium triangular side length]. For the asymmetrical mode, one section through the potential surface along the line  $q = q_1$  has been used [see Fig. 7(a);  $\varphi = 0, \pi$  and  $0 \leq q \leq \infty$ ] and a second one along  $q_2$  [Fig. 7(b);  $\varphi = \pi/2, -\pi/2$  and  $0 \leq q \leq \infty$ ]. Figure 9(b) illustrates the relative motion of the three H nuclei in the  $R$ - $r$  plane, with  $R$  and  $r$  Jacobi coordinates, for the aforementioned vibrational modes (without  $q_2$ ) and shows the ranges of  $R$  and  $r$  for which calculations have been performed.

The upper sheet of the ground state is bonding and therefore carries discrete rovibronic levels with an average lifetime called  $\tau_2$  and Eq. (4) is applicable for transitions starting from  $n=3$  Rydberg states and ending on this upper sheet. Vibrational states on the lower sheet of the ground state are considered quasibound<sup>1</sup> in the region of the saddles and discrete levels there are assumed to have an average lifetime  $\tau_1$  and again Eq. (4) is applied.

<sup>1</sup>‘‘Quasibound’’ in general means that the molecule dissociates after a few periods of vibration. Here dissociation on the lower sheet takes place since the ground-state potential surface of  $H_3$  is bonding in the saddle region only in one direction (compare Fig. 6). On the upper sheet of the potential, it can ‘‘escape’’ quickly through the point of conical intersection.

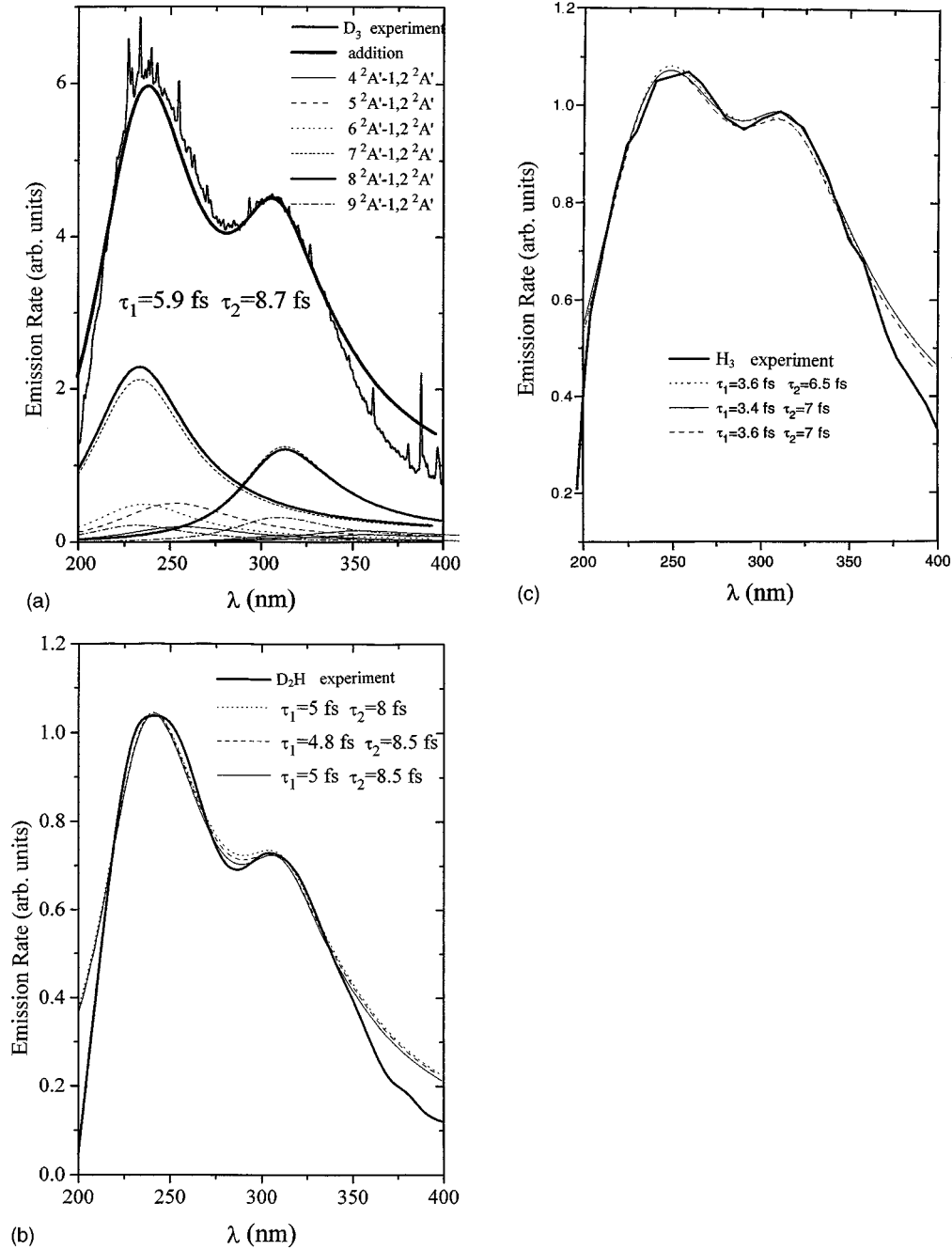


FIG. 10. (a)  $D_3$  uv spectrum (the narrow peaks on top are due to atomic cesium lines, which are also excited when  $D_3^+$  passes through the cesium beam). In addition, the simulation fitted to the experimental spectrum by variation of  $\tau_1$  and  $\tau_2$  is shown. The contributions of individual transitions are also shown at the bottom of the figure. The dominant peaks at 240 and 320 nm originate from transitions between  $3d$  levels (7, 8, and  $9^2A'$ ) and the  $1^2A'$  part and  $2^2A'$  part, respectively, of the ground state. (b) and (c)  $D_2H$  and  $H_3$  spectra and their fits (Cs atomic lines removed and smoothed). The simulated spectrum is shown for different pairs of  $\tau_1, \tau_2$ . The same potentials and electric transition moments were used for the simulation of the experimental spectra of all three isotopomers.

Between the saddles, the lower sheet is purely dissociative (Fig. 6), leading to a continuous energy range  $\Delta E$  of the dissociation products, instead of discrete energy levels. A lifetime can be derived for this part from the expression  $\tau = h/\Delta E$ , with  $h$  Planck's constant, as is shown, for instance, in Ref. [25].<sup>2</sup>

For each individual line of the bound-(quasi)bound transitions a Lorentzian line profile is used whose width is determined by the lifetime  $\tau_1$  or  $\tau_2$ , respectively, so that this contribution to the spectrum becomes

$$I(\omega) = \sum_{e', e'', v', v'', j', j''} \frac{I_{e' e'' v' v'' j' j''}}{2\pi} \times \frac{1/\tau_i}{(\omega - \omega_{e' e'' v' v'' j' j''})^2 + 1/4\tau_i^2}, \quad i=1,2. \quad (6)$$

<sup>2</sup>Here the general definition of a lifetime as discussed in Refs. [24, 25] is always applied.

TABLE VI. Lifetimes  $\tau_1$  and  $\tau_2$  for the lower and upper sheets, respectively of the ground-state hyper-surface of  $\text{H}_3$  and for its isotopomers  $\text{D}_2\text{H}$  and  $\text{D}_3$ . The reduced mass  $\mu$  of each isotopomer is given in the fourth column. In the fifth column the difference between  $\tau_1$  and  $\tau_2$  is listed and the two last columns give the “reduced” lifetimes for the upper and lower sheets, respectively (see the text).

Molecule	$\tau_1$ (fs)	$\tau_2$ (fs)	$\mu$ (a.u.)	$\Delta\tau$ (fs)	$\tau_1/\mu^{1/2}$	$\tau_2/\mu^{1/2}$
$\text{H}_3$	$3.5 \pm 0.5$	$6.7 \pm 0.5$	$\frac{2}{3}$	3.2	4.3	8.2
$\text{D}_2\text{H}$	$4.9 \pm 0.5$	$8.2 \pm 0.5$	$1 \left(\frac{4}{5}, \frac{6}{5}\right)$	3.3	4.9	8.2
$\text{D}_3$	$5.9 \pm 0.5$	$8.7 \pm 0.5$	$\frac{4}{3}$	2.8	5.0	7.6

The lifetimes of the emitting  $n=3$  levels are longer than  $\tau_1$  and  $\tau_2$  by about a factor of  $10^6$  and therefore do not notably contribute to the Lorentzian linewidths. In the case of the bound-free transitions we have to integrate over the continuum  $\Delta E$  without any free parameter. The total uv spectrum was obtained by summing over the contributions from all bound-(quasi)bound and bound-free transitions. The fit to the experimental uv spectrum was achieved by varying only  $\tau_1$  and  $\tau_2$  as fit parameters. The fits were performed for a set of temperatures  $T$  ( $T$  as a parameter) and  $T=1500$  K was found to result in the best fit. At this temperature the population of the first excited vibrational state is about a factor 15 smaller than for the vibrational ground state of the asymmetric mode (vibrational frequency of approximately  $2500 \text{ cm}^{-1}$ ).

When doing the simulation of the spectra separately for the asymmetric and symmetric modes [straight lines labeled (2) and (3) in Fig. 9], it turns out that the radiative decay from Rydberg states into the dissociative asymmetric mode is greatly favored because of large Franck-Condon factors. The contribution from the symmetric mode was found to be smaller by a factor of 20 and was neglected when fitting the spectra.

The results of these fits, i.e., the calculated spectra as fitted to the experimentally observed spectra for three isotopomers are shown in Figs. 10(a), 10(b), and 10(c). Individual contributions of different electronic orbitals are also shown in the lower part of the fitted spectra for the case of  $\text{D}_3$ . Figure 11 demonstrates the sensitivity of the simulations of the spectra to the variation of the lifetimes in the case of  $\text{H}_3$ .

Nearly perfect fits, also in the wavelength region between 320 and 400 nm, were achieved when the line profiles were chosen as sums of Lorentzian and Gaussian line shapes (50:50) as shown in Fig. 12. This is probably due to the fact that the line shapes change from Lorentzian to Gaussian when the potential surface on which the transition ends changes from bonding to dissociative as is the case for the  $\text{H}_3$  ground state [25]: Here the character changes three times from (quasi)bonding to dissociative when  $\varphi$  is varied from 0 to  $2\pi$ , as can be seen in Fig. 6. However, for all numerical results only Lorentzian line shapes were used.

As an additional check, the uv spectrum has also been simulated using reaction (Jacobian) coordinates  $r$ ,  $R$ , and  $\delta$  [see Fig. 9(a) for an illustration of their definition] for the calculation of vibrational wave functions [ $r=1.7$ ,  $\delta=\pi/2$ , and  $1 < R < 3$ ; straight line labeled (1) in Fig. 9(b)]. The quality of the fits performed with reaction coordinates (see Fig. 13) is equivalent to that for the vibrational (asymmetric) coordinates and delivers lifetimes very close to those ob-

tained from the fits shown in Figs. 10(a), 10(b), and 10(c).

If the coupling of the asymmetric modes to the symmetric mode had substantial influence on the spectra and on the lifetimes extracted from the fits, then one would expect to find different results when using the reaction coordinate  $R$  since it is a linear combination of the symmetric and asymmetric coordinates. However, the reaction coordinate calculation gives nearly the same results as the previous calculation using normal vibrational coordinates  $q_0$ ,  $q_1$ , and  $q_2$ .

*A priori*, it is not clear that simulations of the spectra are sufficiently accurate when only cross sections through the potential surfaces are used for the calculation. However, the fact that simulations in two different coordinate systems (orthogonal vibrational coordinates and reaction coordinates) lead to nearly same results in good agreement with experimental spectra supports the validity of this computational approach.

The results for the lifetimes  $\tau_1$  and  $\tau_2$  for the different isotopomers are given in Table VI. To our knowledge, the lifetimes have not been experimentally determined so far and are hard to calculate from first principles. Only two theoretical treatments of them are known to us [26,27].

## V. DISCUSSION OF THE LIFETIMES OF THE GROUND STATE

The potential surface of the ground state of  $\text{H}_3$  on which the elementary chemical reaction between  $\text{H}_2$  and  $\text{H}$  takes place today serves as the prototypical reaction surface in quantum chemistry (e.g., [15–17]). The accuracy of this potential surface is believed to be so high that results of calculations of the dynamics taking place on this surface can be compared directly to experiment.

Recently, various groups have experimentally studied the dynamics on this surface by measuring the product state distribution after scattering of vibrationally and rotationally pre-

TABLE VII. Lifetimes calculated classically. In the calculation of  $\tau_1$  the starting point of the classical particle with reduced mass  $\mu$  on the potential surface is taken to be  $R=1.65a_0$  and the end point is  $R=2.5a_0$ . For  $\tau_2$  the initial separation was  $1.3a_0$ . The fourth column indicates the lifetime one obtains when adding to the classical dissociation time  $\tau_2^{\text{cl}}$  one vibrational period  $T_{\text{osc}}$  on the upper sheet. The result is to be compared to  $\tau_2$  in the last column.

Molecule	$\tau_1^{\text{cl}}$ (fs)	$\tau_2^{\text{cl}}$ (fs)	$\tau_2^{\text{cl}} + T_{\text{osc}}$ (fs)	$\tau_2$ (fs)
$\text{H}_3$	4.3	4.6	$4.6 + 2.1 = 6.7$	$6.7 \pm 0.5$
$\text{D}_2\text{H}$	5.3	5.5	$5.5 + 2.7 = 8.2$	$8.2 \pm 0.5$
$\text{D}_3$	6.2	6.5	$6.5 + 3 = 9.5$	$8.7 \pm 0.5$

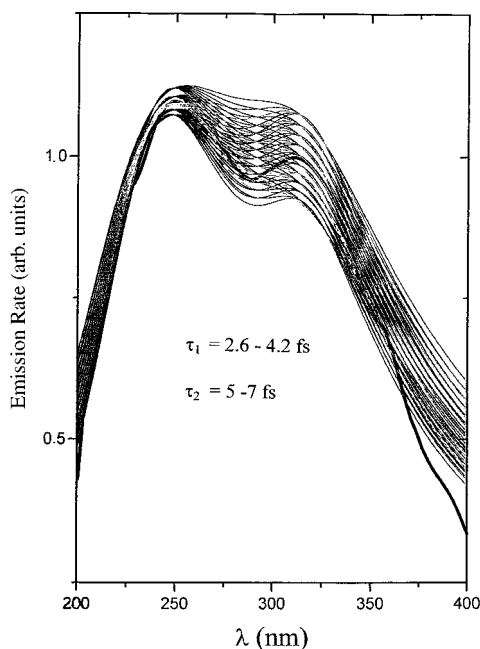


FIG. 11. Sensitivity of the fit to the experimental spectrum of  $H_3$  on the variation of the lifetimes  $\tau_1$  and  $\tau_2$ . The bunch of curves corresponds to the variation of  $\tau_1$  and  $\tau_2$  inside the intervals given in the diagram for them.

pared reactants [28–32]. Nieh and Valentini observed sharp resonances in the partial cross sections  $\sigma(v, j \rightarrow v', j')$  as a function of the relative collision energy of the reactants [28]. They interpreted their results as dynamical resonances due to vibrational modes of the  $H_3$  transition state. Zare and co-workers refuted this interpretation [29,32].

A theoretical treatment of the quasibound states of the transition state and in particular a determination of the life-

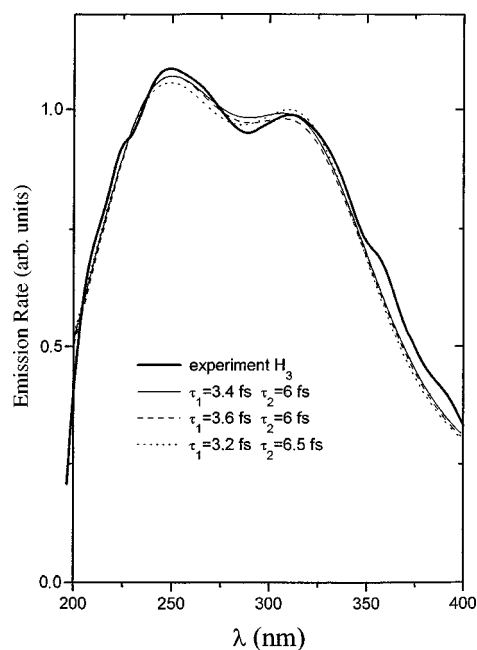


FIG. 12. Simulation of the  $H_3$  spectrum using a mixture of Gaussian and Lorentzian line profiles (see the text).

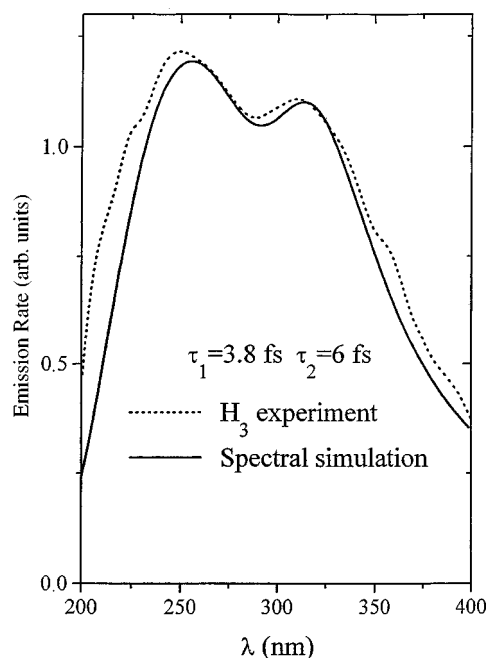


FIG. 13. Simulation of the  $H_3$  spectrum in reaction coordinates.

times on the potential surface was given by Zhao *et al.* [26]. Here we use an alternative method to investigate the  $H_3$  transient ground state: We study the radiative decay of bound excited Rydberg states into this state. A complementary method is to investigate the fragments  $H+H_2$  after predissociation of the  $n=2$  and 3 states due to their coupling to the ground state [33].

Of the three isotopomers investigated, the ground state of  $H_3$  is characterized by the shortest lifetimes:  $\tau_1=3.5$  fs and  $\tau_2=6.7$  fs. These are among the shortest lifetimes ever observed in molecular spectroscopy, i.e., the  $H_3$  ground state is “the most transient of the transient states” as Valentini and Philips noted [34]. Such short lifetimes arise since the small H masses are accelerated on the steep slopes of the  $H_3$  ground-state surface. The lifetimes against dissociation on the ground state quoted here arise from states with angular momentum quantum number  $j$  ranging from 0 to 7 (determined by the initial population of the  $n=3$  states) and vibrational coordinate  $q$  between 0 and  $0.25a_0$ .

The lifetimes of the different isotopomers should increase with the square root of the reduced mass  $\mu$  of the dissociation products. The lifetimes obtained from fits of the experimental spectra reflect this behavior as can be seen from Table VI: The reduced lifetimes  $\tau_1\mu^{-1/2}$  and  $\tau_2\mu^{-1/2}$  are approximately equal for the three isotopomers within the uncertainties of 0.5 fs.

One may also calculate  $\tau_1^{cl}$  and  $\tau_2^{cl}$ , the time a classical particle with mass  $\mu$  would need to slide down the potential of the ground state. Since the magnitude squared of the nuclear wave function of  $H_3$  is small in spatial extent in comparison to the potential surface, one would expect these classical lifetimes (Table VII) to be close to the quantum-mechanical results. Indeed, such a classical trajectory calculation results in a value for  $\tau_1^{cl}$  close to the experimental result. However,  $\tau_2$  is for all isotopomers appreciably longer than the classical value  $\tau_2^{cl}$ , which indicates that the

direct classical path is not taken in the dissociation starting on the upper surface. The difference can be tentatively interpreted as the time spent in vibrational levels of the upper nonadiabatic Jahn-Teller sheet. In fact, if one vibrational period, for example, 2.1 fs for  $\text{H}_3$ , is added to  $\tau_1^{\text{cl}}$  one arrives at our experimental value  $\tau_2$ .

It is interesting to note that  $\tau_1$  (the average lifetime of the quasibound states on the lower sheet; compare Sec. IV B) for all isotopomers turns out to be close to the dissociation lifetime  $\tau = h/\Delta E$  [25], which means that also states close to the saddle parts of the potential dissociate before vibrating.

There are, to our knowledge, no published experimental lifetimes that are directly comparable to the ones presented here. Zhao *et al.* [26] studied ‘‘quasibound states of the transient state’’  $\text{H}_3$  and, for example, calculated the time interval from ‘‘the point when the reactants enter the surface until the appearance of the products in the exit channel.’’ These delay times that lie between 1 and 16 fs for  $0 \leq j \leq 4$  should in principle be observable in scattering experiments. Since we observe ‘‘half collisions,’’ the agreement is satisfactory.

Our results are best compared with the theoretical work of Krause *et al.* [27], who performed quantum-mechanical calculations of the dynamics of the dissociation of  $\text{H}_3$  Rydberg states at total energies up to 6 eV, i.e., far above the conical intersection. Their results show the necessity of including both sheets of the ground-state surface in the dynamics. They found that the square of the autocorrelation function  $\phi(t) = \langle \psi(r,0) | \psi(r,t) \rangle$  ( $\psi$  is the normalized nuclear wave function) goes to zero on the lower sheet within 5 fs and reaches a minimum after 10 fs on the upper sheet. This is in good agreement with our observation.

The lifetime of the upper sheet is determined by both the symmetric decay to  $\text{H}+\text{H}+\text{H}$  and the leakage to the lower sheet through the conical intersection. Therefore, we believe that the importance of our determination also lies in the relative magnitude of the lifetimes  $\tau_1$  and  $\tau_2$ , which represents a measure for the coupling between the upper and lower sheet.

## VI. CONCLUSION

uv spectra of  $\text{H}_3$  and two of its isotopomers have been experimentally observed and could be attributed to transitions from  $n=3$  Rydberg states to the dissociative ground state. Lifetime measurements of the emitting levels facilitated the assignment of the uv spectra (besides the observed

wavelength range). Detailed simulations of the uv spectra of three isotopomers using *ab initio* data for the potential surfaces and electric-dipole transition moments support our previous interpretation of the experimental spectra [8]: The shape of the spectra mainly reflects features of the ground state not observed before in other experiments. The two separate maxima reflect the two Jahn-Teller sheets and the conical intersection. The widths of the maxima indicate extremely short lifetimes in the femtosecond range against dissociation for both sheets of the ground state of  $\text{H}_3$ . Good agreement is found with theoretical work of other authors. The fact that using the same potentials and transition moments delivers good fits for all the isotopomers considered indicates the validity of the Born-Oppenheimer approximation.

The continuous uv spectra only allow us to determine average lifetimes (for different rovibrational states with  $v''=0,1$  and  $j''=0,1,\dots,7$ ) for the two Jahn-Teller sheets. Since the maximum of the population is at  $j''=3,4$ , the lifetimes determined might be close to those of these  $j''$  states.

The technique used here to investigate the ground-state surface can be made more specific with respect to total angular momentum, for example, by state selectively preparing excited bound  $n=3$  states using lasers. Monitoring their radiative decay to the ground state would then open the possibility to probe the dynamics on the ground-state surface for individual angular momentum states. Another possibility to obtain well-defined ‘‘initial conditions’’ on the ground state is to apply stimulated emission pumping from populated excited states into the ground state.

*Note added in proof.* Very recently S. Mahapatra and H. Köppel of the University of Heidelberg performed a quantum-mechanical wave packet *ab initio* calculation of our uv spectra, which included nonadiabatic coupling in the ground-state potential. Their calculations reproduce most of the features of our spectra [35].

## ACKNOWLEDGMENTS

D.A. is very grateful for financial support from the Alexander von Humboldt Foundation. We thank T. W. Hänsch for stimulating discussions and acknowledge the indispensable technical help of W. Simon, K. Linner, and H. Brückner.

- 
- [1] G. Herzberg, *J. Chem. Phys.* **70**, 4806 (1979).  
 [2] I. Dabrowski and G. Herzberg, in *Amazing Light: A Festschrift for Charles Townes' 80th Birthday*, edited by Raymond Chiao (Springer-Verlag, Berlin, in press).  
 [3] H. Figger, M. N. Dixit, R. Maier, W. Schrepp, H. Walther, I. R. Peterkin, and J. K. G. Watson, *Phys. Rev. Lett.* **52**, 906 (1984); H. Figger, Y. Fukuda, W. Ketterle, and H. Walther, *Can. J. Phys.* **62**, 1274 (1984).  
 [4] I. Dabrowski and G. Herzberg, *Can. J. Phys.* **58**, 1238 (1980).  
 [5] G. Herzberg and J. K. G. Watson, *Can. J. Phys.* **58**, 1250 (1980).  
 [6] G. Herzberg, H. Lew, J. J. Sloan, and J. K. G. Watson, *Can. J. Phys.* **59**, 428 (1981).  
 [7] A. B. Raksit, R. F. Porter, W. P. Garver, and J. J. Leventhal, *Phys. Rev. Lett.* **55**, 378 (1985).  
 [8] R. Bruckmeier, Ch. Wunderlich, and H. Figger, *Phys. Rev. Lett.* **72**, 2550 (1994).  
 [9] H. Figger, W. Ketterle, and H. Walther, *Z. Phys. D* **13**, 129 (1989).  
 [10] W. Ketterle, H. Figger, and H. Walther, *Z. Phys. D* **13**, 139 (1989).  
 [11] Ch. Wunderlich, V. Betz, R. Bruckmeier, and H. Figger, *J. Chem. Phys.* **98**, 9362 (1993).  
 [12] Ch. Wunderlich, B. Witzel, R. Bruckmeier, and H. Figger, *Can. J. Phys.* **72**, 1236 (1994).

- [13] R. Bruckmeier, Ch. Wunderlich, and H. Figger, *Phys. Rev. A* **52**, 334 (1995).
- [14] H. Eyring and M. Polanyi, *Z. Phys. Chem. Abt. B* **12**, 279 (1931).
- [15] P. Siegbahn and B. Liu, *J. Chem. Phys.* **68**, 2457 (1978).
- [16] D. G. Truhlar and C. J. Horowitz, *J. Chem. Phys.* **68**, 2466 (1979).
- [17] R. N. Porter and M. Karplus, *J. Chem. Phys.* **40**, 1105 (1964); R. N. Porter, R. M. Stevens, and M. Karplus, *ibid.* **49**, 5163 (1968).
- [18] See, for instance, W. E. Ernst and S. Rakowsky, *Phys. Rev. Lett.* **74**, 58 (1995).
- [19] H. F. King and K. Morokuma, *J. Chem. Phys.* **71**, 3213 (1979).
- [20] I. D. Petsalakis, G. Theodorakopoulos, and J. S. Wright, *J. Chem. Phys.* **89**, 6850 (1988).
- [21] R. J. Buenker, in *Studies in Physical and Theoretical Chemistry (Current Aspects of Quantum Chemistry 1981)*, edited by R. Carbo (Elsevier, Amsterdam, 1982), Vol. 21; R. J. Buenker and R. A. Philips, *J. Mol. Struct.* **123**, 291 (1985).
- [22] See, for instance, G. Herzberg, *Molecular Spectra and Molecular Structure, Spectra of Diatomic Molecules* (Van Nostrand Reinhold, New York, 1950), pp. 426 and 200, Eq. 4.74; see also L. D. Landau and E. M. Lifshitz, *Quantum Mechanics* (Nauka, Moscow, 1974), Chap. 5; J. Tellinghuisen, in *Photodissociation and Photoionisation*, edited by K. P. Lawley (Wiley, New York, 1985).
- [23] J. W. Cooley, *Math. Comput.* **15**, 363 (1961).
- [24] C. Cohen-Tannoudji, B. Diu, and F. Laloe, *Quantum Mechanics* (Wiley, New York, 1977).
- [25] Reinhard Schinke, *Photodissociation Dynamics* (Cambridge University Press, Cambridge, 1993), pp. 109–133.
- [26] M. Zhao, M. Mladenovic, D. G. Trular, D. W. Schwenke, O. Sharafeddin, Y. Sun, and D. J. Kouri, *J. Chem. Phys.* **91**, 5302 (1989).
- [27] J. L. Krause, K. C. Kulander, J. C. Light, and A. E. Orel, *J. Chem. Phys.* **96**, 4283 (1992); A. E. Orel and K. C. Kulander, *ibid.* **91**, 6086 (1989).
- [28] J. C. Nieh and J. J. Valentini, *J. Chem. Phys.* **92**, 1083 (1990).
- [29] D. E. Adelman, N. E. Shafer, D. A. V. Kliner, and R. N. Zare, *J. Chem. Phys.* **97**, 7323 (1992).
- [30] L. Schnieder, W. Meier, K. H. Welge, M. N. R. Ashfold, and C. M. Western, *J. Chem. Phys.* **92**, 7027 (1992).
- [31] L. Schnieder, K. Seekamp-Rahn, J. Borkowski, E. Wrede, K. H. Welge, F. J. Aoiz, L. Banares, M. J. D’Mello, V. J. Herrero, V. Saez Rabanos, and R. E. Wyatt, *Science* **29**, 207 (1995).
- [32] D. A. V. Kliner, D. E. Adelman, and R. N. Zare, *J. Chem. Phys.* **94**, 1069 (1991).
- [33] P. C. Cosby and H. Helm, *Phys. Rev. Lett.* **61**, 298 (1988).
- [34] J. J. Valentini and D. L. Philips, in *Advances in Gas Phase Photochemistry and Kinetics*, edited by M. N. R. Ashfold and J. E. Bagold (Royal Society of Chemistry, London, 1989).
- [35] S. Mahapatra and H. Köppel (unpublished).